Electronic Supplementary Material (ESI) for Soft Matter.
This journal is © The Royal Society of Chemistry 2019

Soft Matter

ARTICLE TYPE

Cite this: DOI: 10.1039/xxxxxxxxxx

Supplementary Information for: Poroelasticity of (bio)polymer networks during compression: theory and experiment

Melle T.J.J.M. Punter,*[a] Bart E. Vos,*[bc] Bela M. Mulder,[a] and Gijsje H. Koenderink[bd‡]

In this Supplementary Information we first present in section S1 our approximate solution to the poroelastic equations of motion, equation (1)–(3) in the manuscript. Afterwards, we treat the assumptions on which the approximate form of the poroelastic equations is based, as well as the assumptions underlying our solution. Next, we consider in section S2 the cubic lattic model used to estimate the dependence of the permeability k of a fibrin network on the concentration of fibrinogen c and the compressive strain ϵ. In section S3, we present the fit results of the measured normal force in all compression experiments and discuss them systematically.

S1 Approximate solution

The approximate closed-form solution to the poroelastic equations of motion is found as an exact solution to an approximate form of the poroelastic equations. First, we state this exact solution. Afterwards, we motivate the approximate form of the poroelastic equations, and detail the underlying assumptions.

We consider the ramp compression of a cylindrical gel bonded to the plates of a parallel-plate rheometer, where the gel network is treated as a linear elastic solid with shear modulus G and bulk modulus K, see Figure S1 and Figure 2 of the manuscript. The gel network has a permeability k, the fluid has dynamic viscosity η, and the gel is compressed at a strain rate $\dot{\epsilon} \equiv v/h$, with v the velocity of the upper plate. Before compression, the gel has an axial length h, a radius a and a large aspect ratio $S \equiv a/h \gg 1$, see Figure S1A. The solution of the exact poroelastic equations, equation (1)–(3) of the manuscript, can be specified by the displacement field of the gel network $\boldsymbol{U}$, the velocity field of the fluid $\boldsymbol{v}_\mathrm{f}$ and the fluid pressure p. For notational convenience, however, we do not use the fluid velocity, but the volume-averaged local velocity of the gel $\boldsymbol{V} \equiv \phi_\mathrm{n}\boldsymbol{v}_\mathrm{n} + \phi_\mathrm{f}\boldsymbol{v}_\mathrm{f}$ instead, with $\phi_\mathrm{f}(\phi_\mathrm{n})$ the volume fraction and $\boldsymbol{v}_\mathrm{f}(\boldsymbol{v}_\mathrm{n} \equiv \partial_t \boldsymbol{U})$ the velocity field of the fluid(gel network). In the exact solution of the approximate form of the poroelastic equations, for any radial position r, vertical position z and time t with $(r, z, t) \in]0, a] \times [0, h] \times [0, \infty]$, the displacement field of the gel network $\boldsymbol{U}(r, z, t) = U(r, z, t)\hat{\boldsymbol{r}} + W(z, t)\hat{\boldsymbol{z}}$, with $U(r, z, t)$ the radial displacement and $W(z, t)$ the vertical displacement, reads the following

$$U(r, z, t) = T(t)\dot{\epsilon}t_\perp \frac{r}{4}\frac{z}{h}\left(1 - \frac{z}{h}\right), \tag{S1}$$

$$W(z, t) = -(1 - T(t))\,\epsilon z\frac{z}{h}\left(3 - 2\frac{z}{h}\right) - T(t)\epsilon z + T^2(t)\dot{\epsilon}t_\perp \frac{h}{12}\frac{M - G}{M}\left(\frac{z}{h} - 3\left(\frac{z}{h}\right)^2 + 2\left(\frac{z}{h}\right)^3\right), \tag{S2}$$

$$T(t) = 1 - \exp\left(-12\frac{t}{t_\perp}\right), \tag{S3}$$

where $t_\perp \equiv \eta h^2/Gk$ is the time for the gel to become pressurized, i.e., $\partial_t p = 0$, during compression, $\epsilon = \dot{\epsilon}t$ is the compressive strain on the gel, $M = K + 4G/3$ is the longitudinal modulus, and $T(t)$ is the transition function which brings the gel from volume-conserving compression into the pressurized phase. The fluid pressure $p(r, z, t)$ is given by

$$p(r, z, t) = T(t)G\frac{S^2}{4}\dot{\epsilon}t_\perp\left(1 - \left(\frac{r}{a}\right)^2\right) + 2\,(1 - T(t))\,G\epsilon + p_\mathrm{ext} - 6\frac{z}{h}\left(1 - \frac{z}{h}\right)\left[(1 - T(t))\,M\epsilon + \left(T^2(t) - T(t)\right)\frac{M - G}{12}\dot{\epsilon}t_\perp\right], \tag{S4}$$

where p_ext is the pressure of the fluid in which the gel is immersed, and the volume-averaged local velocity of the gel $\boldsymbol{V}(r, z, t)$ is found as

$$\boldsymbol{V}(r, z, t) = (1 - T(t))\,\boldsymbol{V}^\mathrm{vc}(r, z) + T(t)\boldsymbol{V}^\mathrm{cp}(r, z), \tag{S5}$$

$$\boldsymbol{V}^\mathrm{vc}(r, z) = 3\dot{\epsilon}r\frac{z}{h}\left(1 - \frac{z}{h}\right)\hat{\boldsymbol{r}} - z\dot{\epsilon}\frac{z}{h}\left(3 - 2\frac{z}{h}\right)\hat{\boldsymbol{z}}, \tag{S6}$$

$$\boldsymbol{V}^\mathrm{cp}(r, z) = \frac{r}{2}\dot{\epsilon}\hat{\boldsymbol{r}} - z\dot{\epsilon}\hat{\boldsymbol{z}}, \tag{S7}$$

* These authors contributed equally to this work.
[a] AMOLF, Theory of Biomolecular Matter, Science Park 104, 1098XG Amsterdam, the Netherlands
[b] AMOLF, Biological Soft Matter, Science Park 104, 1098XG Amsterdam, the Netherlands
[c] Current address: ZMBE, Mechanics of cellular systems Group, Institute of Cell Biology, Westfälische Wilhelms-Universität, Von-Esmarch-Straße 56, 48149 Münster, Germany.
[d] Current address: Department of Bionanoscience, Kavli Institute of Nanoscience Delft, Delft University of Technology, 2629HZ Delft, The Netherlands
‡ Corresponding Author, email: G.Koenderink@amolf.nl

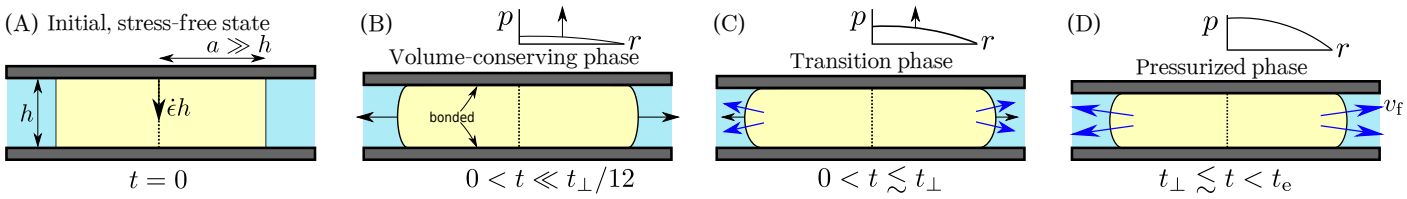

Fig. S1 The compression phases of (**A**) an initially stress-free cylindrical fibrin gel (yellow) of radius a and height h with high aspect ratio $S \equiv a/h \gg 1$ (Figure not on scale). The gel is ramp compressed in a parallel-plate rheometer with the upper plate (gray) having a constant velocity $\dot{\epsilon}h$, where $\dot{\epsilon}$ is the strain rate. **B**) Compression commences with the volume-conserving phase. The fibrin network starts to bulge out (black arrows) because the gel is bonded to the plates, causing the fluid pressure p to build up. **C** The build-up proceeds, causing a fluid outflow velocity v_f (blue arrows) due to the fluid pressure gradient, $v_f \propto -\partial p/\partial r$ with r the radial coordinate in the fibrin gel. After the pressurizing time $t_\perp$, the outward bulging of the gel network, which induces the fluid pressure, stabilizes. **C**) In the pressurized phase, the gel is compressed further at maximal fluid pressure until at time t_e the compression stops.

which shows that the volume averaged local velocity of the gel transitions between that of volume-conserving compression $\boldsymbol{V}^{\rm vc}(r,z,t)$ and that in the pressurized phase $\boldsymbol{V}^{\rm cp}(r,z,t)$ where the fluid pressure is constant in time.

Equation (S1)–(S7) exactly solve the following approximate set of poroelastic bulk and boundary equations of motion: equation (S8)–(S17). First of all, equation (S1)–(S4) solve the exact overall force balance, see equation (1) of the manuscript, which reads

$$\frac{\partial p}{\partial r} = M\frac{\partial}{\partial r}\frac{1}{r}\frac{\partial rU}{\partial r} + (M-G)\frac{\partial^2 W}{\partial r \partial z} + G\frac{\partial^2 U}{\partial z^2}, \tag{S8}$$

$$\frac{\partial p}{\partial z} = M\frac{\partial^2 W}{\partial z^2} + (M-G)\frac{1}{r}\frac{\partial}{\partial r}r\frac{\partial U}{\partial z} + G\frac{1}{r}\frac{\partial}{\partial r}r\frac{\partial W}{\partial r}. \tag{S9}$$

Equation (S1)–(S7) solve an approximate form of Darcy's law, see equation (3) in the manuscript, which has been rewritten using the definition of the volume averaged local velocity of the gel $\boldsymbol{V} \equiv \phi_{\rm n}\boldsymbol{v}_{\rm n} + \phi_{\rm f}\boldsymbol{v}_{\rm f}$

$$v_{{\rm n},r} - V_r = \frac{k}{\eta}\frac{\partial p}{\partial r}, \tag{S10}$$

$$\langle v_{{\rm n},z} - V_z\rangle = \frac{k}{\eta}\left\langle\frac{\partial p}{\partial z}\right\rangle, \tag{S11}$$

where $\langle X\rangle \equiv (1/h)\int_0^h {\rm d}z\, X$ is the average of X over the axial height of the gel. This form of Darcy's law, which stems from the force balance of the fluid, is approximate because it requires Darcy's law in the vertical direction to be obeyed only on average. Finally, equation (S5)–(S7) solve the incompressibility condition of the gel which follows from mass conservation

$$\nabla\cdot\boldsymbol{V} = 0. \tag{S12}$$

The solution in equation (S1)–(S3) obeys the following essential boundary conditions. Ramp compression and the binding of the gel network to the rheometer plates impose

$$W = 0 \text{ and } V_z = 0, \text{ at } z = 0, \tag{S13}$$

$$W = -\epsilon h \text{ and } V_z = -\dot{\epsilon}h, \text{ at } z = h, \tag{S14}$$

$$U = 0, \text{ at both } z = 0 \text{ and } z = h. \tag{S15}$$

At the free boundary the solution obeys the average form of the tangential overall stress balance, and an approximate form of the radial overall stress balance combined with the permeability condition

$$\langle\sigma'_{rz}\rangle = 0 \text{ at } r = a, \tag{S16}$$

$$\langle\sigma'_{rr}\,(1-T(t)) - p\rangle = -p_{\rm ext}, \text{ at } r = a, \tag{S17}$$

where $\boldsymbol{\sigma'}$ is the Terzaghi effective stress of the gel network, taken to be that of a linear elastic solid.

The time-dependent normal force $F(t)$ on the plates which is generated by the gel during compression, can be calculated from the overall stress at the gel-plate interface as

$$F(t) = -\int_0^a {\rm d}r\, 2\pi r\,(\sigma'_{zz} - p)\Big|_{z=0,h}, \tag{S18}$$

which gives with equation (S1)–(S4)

$$\frac{F(t)}{\pi a^2} = T(t)\left[G\left(\frac{S^2}{8} - T(t)\frac{M-G}{12G}\right)\dot{\epsilon}t_\perp + M\epsilon\right] + (1-T(t))\,2G\epsilon. \tag{S19}$$

The condition for the validity of the solution presented in equation (S1)–(S7) is that $M/GS^2 \ll 1$. Using this validity condition, the dominant part of equation (S19) gives equation (4) of the manuscript.

S1.1 Assumptions

To study the ramp compression of a bonded disk-like gel, we make several assumptions by comparing the bonded gel with a frictionless gel having no friction with the plates of the rheometer. Similar to a frictionless gel, we assume the bonded gel to deform in a volume-conserving manner when compression commences, see Figure S1B. Also similar to a frictionless gel, the fluid pressure is assumed to reach a maximal value during compression, the gel is then pressurized, see Figure S1D. Finally, the gel transitions in the pressurizing time from the volume-conserving to the pressurized phase in a simple mono-exponential time-dependent fashion, see Figure S1C.

S1.1.1 The pressurized phase

Consider a cylindrical gel under compression identical to the case we treat in the manuscript, see Figure S1, but instead of being

This journal is © The Royal Society of Chemistry [year]

bonded to the plates, it experiences no friction with the plates. In this case, the exact solution of the poroelastic equations of motion, equation (1)–(3) in the manuscript, is known[1]. During sufficiently slow ramp compression, the frictionless gel becomes pressurized, i.e., $\partial_t p = 0$, after a pressurizing time $t_\parallel = a^2\eta/kM$. When pressurized, the exact solution for the displacement field, the volume-averaged velocity field and the fluid pressure p of the frictionless gel reads

$$U(r,t) = \nu r\epsilon + a\frac{\eta\dot{\epsilon}a^2}{8kM}\left(\frac{1}{2}-\nu\right)\left((3-2\nu)\frac{r}{a} - \left(\frac{r}{a}\right)^3\right), \tag{S20}$$

$$W(z,t) = -z\epsilon, \tag{S21}$$

$$\boldsymbol{V}(r,z) = \frac{r}{2}\dot{\epsilon}\hat{\boldsymbol{r}} - z\dot{\epsilon}\hat{\boldsymbol{z}}, \tag{S22}$$

$$p(r) = \frac{\eta\dot{\epsilon}}{2k}\left(\frac{1}{2}-\nu\right)\left(a^2 - r^2\right) + p_{\text{ext}}, \tag{S23}$$

which shows that the gel deformation differs from that of a static frictionless solid by an inhomogeneous radial strain proportional to the compression rate, see equation (S20). This inhomogeneous strain causes stress in the gel network, which in turn sources the fluid pressure p required for the outflow of fluid from the gel, see equation (S8) and (S9). The fact that this fluid pressure is constant in time, implies a constant outflow of fluid from the gel, which brings us to the first assumption.

Assumption 1: similar to a frictionless gel, a bonded gel becomes pressurized, i.e., $\partial_t p = 0$, after some pressurizing time $t_\perp$, see Figure S1D.

Given this assumption, we can write down the following approximate solution for a bonded gel in the pressurized phase with constant pressure, which obeys the exact form of equation (S8)–(S15)

$$U^{\text{cp}}(r,z) = \dot{\epsilon}t_\perp\frac{r}{4}\frac{z}{h}\left(1-\frac{z}{h}\right), \tag{S24}$$

$$W^{\text{cp}}(z,t) = -\epsilon z + \dot{\epsilon}t_\perp\frac{h}{4}\frac{1}{6(1-\nu)}\left(\frac{z}{h} - 3\left(\frac{z}{h}\right)^2 + 2\left(\frac{z}{h}\right)^3\right), \tag{S25}$$

$$\boldsymbol{V}^{\text{cp}}(r,z) = \frac{r}{2}\dot{\epsilon}\hat{\boldsymbol{r}} - z\dot{\epsilon}\hat{\boldsymbol{z}}, \tag{S26}$$

$$p(r) = G\frac{S^2}{4}\dot{\epsilon}t_\perp\left(1-\left(\frac{r}{a}\right)^2\right) + p_{\text{ext}}, \tag{S27}$$

where we note that in the bonded case the vertical strain is inhomogeneous instead of the radial strain in the frictionless case, and we used the permeability condition $p = p_{\text{ext}}$ at the free boundary $r = a$. The volume-averaged gel velocity field $\boldsymbol{V}^{\text{cp}}$ equals that of a frictionless volume-conserving solid because $\partial_t U = 0$, implying all radial motion is due to fluid flow. The velocity field of the fluid equals that of a frictionless volume-conserving solid, because it is not bonded to the rheometer plates and flows through the radially static, but vertically comoving, gel network.

To study whether this approximate solution is reasonable, we consider the exact form of the bulk equations of motion, equation (S8)–(S12), giving

$$\frac{\eta}{k}\left(\frac{\partial U}{\partial t} - V_r\right) = M\frac{\partial}{\partial r}\frac{1}{r}\frac{\partial rU}{\partial r} + (M-G)\frac{\partial^2 W}{\partial r\partial z} + G\frac{\partial^2 U}{\partial z^2}, \tag{S28}$$

$$\frac{\eta}{k}\left(\frac{\partial W}{\partial t} - V_z\right) = M\frac{\partial^2 W}{\partial z^2} + (M-G)\frac{1}{r}\frac{\partial}{\partial r}r\frac{\partial U}{\partial z} + G\frac{1}{r}\frac{\partial}{\partial r}r\frac{\partial W}{\partial r}, \tag{S29}$$

$$\nabla\cdot\boldsymbol{V} = 0, \tag{S30}$$

where we eliminated the fluid pressure p. The boundary conditions (BCs) are equations (S13)–(S15), combined with the exact boundary conditions at the free boundary: the overall force balance and the permeability condition

$$\sigma'_{rr} - p = -p_{\text{ext}}, \text{ at } r = a, \tag{S31}$$

$$\sigma'_{rz} = 0, \text{ at } r = a, \tag{S32}$$

$$p = p_{\text{ext}}, \text{ at } r = a, \tag{S33}$$

where equation (S31) is the overall balance of forces perpendicular to the free boundary, equation (S32) is the overall balance of forces tangential to the free boundary, and equation (S33) expresses that the gel network is permeable for fluid.

The exact solution in the constant pressure phase can be written as $\boldsymbol{U} = \boldsymbol{U}^{\text{cp}} + \Delta\boldsymbol{U}$ and $\boldsymbol{V} = \boldsymbol{V}^{\text{cp}} + \Delta\boldsymbol{V}$, with $\Delta\boldsymbol{U}$ and $\Delta\boldsymbol{V}$ the difference solution, i.e., the difference between the exact and the approximate solution in the pressurized phase. To show that the difference may be negligible, we scale all quantities to their presumed typical sizes: $\tilde{U} = \Delta U/h$, $\tilde{W} = \Delta W/h$, $\tilde{V}_r = \Delta V_r/(a/t_{\text{ext}})$, $\tilde{V}_z = \Delta V_z/(h/t_{\text{ext}})$, $\xi = z/h$, $\rho = r/a$, $\tau_{\text{ext}} = t/t_{\text{ext}}$ and we define t_{ext} as the externally determined time scale of ramp compression, $t_{\text{ext}} \sim h/v$ with v the velocity of the upper plate. The bulk equations of motion for the difference solution read

$$\frac{\partial\tilde{U}}{\partial\tau_{\text{ext}}} - S\tilde{V}_r = \frac{t_{\text{ext}}}{t_\perp}\left(\frac{M}{GS^2}\frac{\partial}{\partial\rho}\frac{1}{\rho}\frac{\partial\rho\tilde{U}}{\partial\rho} + \frac{M-G}{GS}\frac{\partial^2\tilde{W}}{\partial\rho\partial\xi} + \frac{\partial^2\tilde{U}}{\partial\xi^2}\right), \tag{S34}$$

$$\frac{\partial\tilde{W}}{\partial\tau_{\text{ext}}} - \tilde{V}_z = \frac{t_{\text{ext}}M}{t_\perp G}\left(\frac{\partial^2\tilde{W}}{\partial\xi^2} + \frac{1-\frac{G}{M}}{S}\frac{1}{\rho}\frac{\partial}{\partial\rho}\rho\frac{\partial\tilde{U}}{\partial\xi} + \frac{G}{MS^2}\frac{1}{\rho}\frac{\partial}{\partial\rho}\rho\frac{\partial\tilde{W}}{\partial\rho}\right), \tag{S35}$$

$$\tilde{\nabla}\cdot\tilde{\boldsymbol{V}} = 0, \tag{S36}$$

where $t_\perp = h^2\eta/kG$ is the pressurizing time, and the boundary conditions read

$$\tilde{W} = 0, \tilde{V}_z = 0 \text{ and } \tilde{U} = 0, \text{ at both } \xi = 0 \text{ and } \xi = 1, \tag{S37}$$

$$M\frac{\partial\tilde{U}}{\partial\rho} + \Lambda\frac{\tilde{U}}{\rho} = -S\Big(\Lambda\frac{\partial\tilde{W}}{\partial\xi} + \Lambda\Big\{-\epsilon + \frac{\dot{\epsilon}t_\perp}{24(1-\nu)}\Big[1-6\left(\frac{z}{h} - \left(\frac{z}{h}\right)^2\right)\Big]\Big\} + (M+\Lambda)\frac{\dot{\epsilon}t_\perp}{4}\left\{\frac{z}{h} - \left(\frac{z}{h}\right)^2\right\}\Big), \text{ at } \rho = 1, \tag{S38}$$

$$\frac{\partial \tilde{W}}{\partial \rho} = -S\left(\frac{\partial \tilde{U}}{\partial \xi} + \dot{\epsilon} t_\perp \frac{r}{4h}\left\{1 - 2\frac{z}{h}\right\}\right), \text{ at } \rho = 1. \tag{S39}$$

If we assume that $M/GS^2 \ll 1$, then the $M\partial_r(1/r)\partial_r rU$ term is much smaller than the $G\partial_z^2 U$ term, compare equation (S28) to equation (S34), and the $G(1/r)\partial_r r\partial_r W$ term is much smaller than the $M\partial_z^2 W$ term since $G < M$, compare equation (S29) to equation (S35). Neglecting the small terms, both equation (S34) and (S35) are only first order in r instead of second order. The boundary conditions for U and W at $r = 0$ are imposed by smoothness and symmetry: $U = 0$ and $\sigma_{rz} = 0 \implies \partial_r W = 0$ at $r = 0$, and can not be ignored. Therefore, we must neglect the Robin boundary condition for U at $r = a$ in equation (S38), and the Neumann boundary condition for W at $r = a$ in equation (S39). Then, it follows that there are no sources for a nontrivial solution to equation (S34)–(S37), implying that $\tilde{\boldsymbol{U}} = 0$ and $\tilde{\boldsymbol{V}} = 0$ is the solution. Therefore, the approximate solution in equation (S24)–(S26) is expected to be accurate in the pressurized phase, provided that $M/GS^2 \ll 1$.

The neglect of the two small terms is equivalent to treating the dependencies of $\tilde{\boldsymbol{U}}$ and $\tilde{\boldsymbol{V}}$ to the radial coordinate r as static. In fact, the relative size of the different network stress terms, provided $M/GS^2 \ll 1$, holds during the whole of compression, which gives the full time-dependent approximate solution, contained in equation (S1),(S2) and (S5)–(S7) a static dependence on r: $U(r,z,t) \propto r^1$, $W(z,t) \propto r^0$, $V_r(r,z,t) \propto r^1$ and $V_z(z,t) \propto r^0$ for all times t.

Physically, the condition for the approximate solution to hold, $M/GS^2 \ll 1$, means that the radial force in the gel network due to bending of the gel network, sourced by $G\partial_z^2 U$, is much greater than the radial force due to inhomogeneity in the radial strain, sourced by $M\partial_r(1/r)\partial_r rU$. That is, the shear stress induced by friction between the gel and the rheometer plate dominates the network stress in the gel. Similarly, the vertical force in the gel network due to inhomogeneity in the vertical strain, sourced by $M\partial_z^2 W$, is much greater than the vertical force induced by vertical out of plane displacements, sourced by $G(1/r)\partial_r r\partial_r W$. The term $(M - G)\partial_z\partial_r W$ can be smaller or comparable to the $G\partial_z^2 U$ term, depending on the size of the aspect ratio $S \gg 1$, likewise for the size of $(M - G)(1/r)\partial_r r\partial_z U$ relative to $M\partial_z W$. Finally, it should be noted that although the presumed magnitude of U, which we take to be h, is uncertain, this presumption does not influence the condition to neglect the radial inhomogeneity term, because the shear stress term, relative to which the radial inhomogeneity term is small, also scales with U.

S1.1.2 The volume-conserving phase

Next, we consider that in the frictionless case[1] for short times after the commencement of compression, i.e., $\pi^2 t/t_\parallel \ll 1$ with $t_\parallel$ the pressurizing time, the gel deforms to good approximation as a volume-conserving frictionless solid, because the outflow of fluid from the gel network is still small. Again, assuming the bonded case to behave analogous to the frictionless case, we arrive at the second assumption.

Assumption 2: similar to a frictionless gel, for times much shorter than the, yet to be determined, pressurizing time $t_\perp$, a bonded gel deforms like a bonded volume-conserving solid, see Figure S1B.

The (quasi)-static displacement field of a volume-conserving linear elastic solid bonded to the plates is[2]

$$U^{\text{vc}}(r,z,t) = 3\epsilon r\frac{z}{h}\left(1 - \frac{z}{h}\right), \tag{S40}$$

$$W^{\text{vc}}(z,t) = -z\epsilon\frac{z}{h}\left(3 - 2\frac{z}{h}\right), \tag{S41}$$

which gives equation (S8) and (S9) in dimensionless form as

$$\frac{\partial \tilde{p}}{\partial \rho} = -6S^2\epsilon\rho, \tag{S42}$$

$$\frac{\partial \tilde{p}}{\partial \xi} = -6\epsilon(1 - 2\xi), \tag{S43}$$

where we defined $\tilde{p} = p/G$. As $S \gg 1$, the majority of the pressure builds up radially, stemming from the $G\partial_z^2 U^{\text{vc}}$ term in equation (S8). This term quantifies the stress induced by bending of the gel network, which is imposed by the binding of the network to the plates. At $z = 0$ and $z = h$, we find that $\partial p/\partial z \neq 0$, however, which implies with Darcy's law, see equation (3) of the manuscript, a vertical flow of fluid relative to the gel network through the impermeable plates of the rheometer. As this would render the plates permeable, we adopt an approximative form of the vertical part of Darcy's law, see equation (S11), by requiring it to hold only when averaged over the axial height of the gel.

S1.1.3 Transition from the volume-conserving phase to the pressurized phase

The frictionless gel transitions from volume-conserving compression to the pressurized phase on a pressurizing time scale $t_\parallel$[1]. Also, previous work in the context of gel compression demonstrated mono-exponential time-dependence, see equation (32) in Yamaue *et al.*[3]. This brings us to the final assumption

Assumption 3: we assume the time-dependent dynamics of the radial displacement of the gel network, transitioning from volume-conserving deformation to the pressurized phase, to be proportional to a transition function $T(t)$, see Figure S1C.

We write $U(r,z,t) = T(t)U^{\text{cp}}$, such that $T(t) \approx 1$ if $t \gtrsim t_\perp$ with $t_\perp$ the pressurizing time, and $T(0) = 0$, because at $t = 0$ we assume the gel to be stress-free. Then, we assume that $\boldsymbol{V}(r,z,t)$, see equation (S5), interpolates between the volume-conserving velocity field of a bonded solid $\boldsymbol{V}^{\text{vc}}(r,z,t)$, see the time-derivative of equation (S40) and (S41), and the volume-conserving velocity field of a frictionless solid $\boldsymbol{V}^{\text{cp}}(r,z,t)$, see equation (S26). The exact radial force balance, equation (S8) combined with equation (S10), can than be solved for $T(t)$, giving the transition function $T(t)$, see equation (S3), along with the pressurizing time $t_\perp = h^2\eta/kG$. Then, by requiring also $W(z,t)$ and $p(r,z,t)$ to transition from their volume-conserving form to their form in the pressurized phase, using only $T(t)$, we obtain as a solution to equation (S8)–(S15) the solution contained in equation (S1)–(S7), but slightly more

This journal is © The Royal Society of Chemistry [year]

general with

$$W(z,t) = -(1-T(t))\,\epsilon z\frac{z}{h}\left(3-2\frac{z}{h}\right) - T(t)\epsilon z + T^n(t)\dot{\epsilon}t_\perp\frac{h}{12}\frac{M-G}{M}\left(\frac{z}{h}-3\left(\frac{z}{h}\right)^2+2\left(\frac{z}{h}\right)^3\right), \tag{S44}$$

$$p(r,z,t) = T(t)G\frac{S^2}{4}\dot{\epsilon}t_\perp\left(1-\left(\frac{r}{a}\right)^2\right) + C - 6\frac{z}{h}\left(1-\frac{z}{h}\right)\left[(1-T(t))\,M\epsilon + \left(T^n(t)-T(t)\right)\frac{M-G}{12}\dot{\epsilon}t_\perp\right], \tag{S45}$$

where $n \geq 2$, and C is an integration constant. The non-uniqueness of this solution, illustrated by the arbitrariness of n, may be related to the approximate nature of the equations of motion it solves.

The terms proportional to $T^n(t)$ are related to the inhomogeneous vertical strain in the pressurized phase, compare equation (S25) to equation (S44). This inhomogeneous vertical strain balances the $(M-G)(1/r)\partial_r r\partial_z U$ term in equation (S29), which measures the local increase in vertical force on the gel network due to the radial change in the deflection of the gel network. If we consider the vertical force balance with the exact form of Darcy's law, and plug in equation (S1), (S5)–(S7), and (S44), we find that the left hand side can be grouped in terms proportional to $T(t)^0, T(t)^1, T(t)^{n-1}$ and $T(t)^n$, whereas the right hand side can be grouped in terms proportional to $T(t)^0, T(t)^1$ and $T(t)^n$. We then set the value of $n \geq 2$ by requiring the dependencies on the transition function $T(t)$ on both sides of the exact equation to match: for each term on the left hand side proportional to $T(t)^m$, there should be a term on the right hand side also proportional to $T(t)^m$. This requirement uniquely sets $n = 2$.

Finally, to determine the integration constant C for the fluid pressure p, we consider the force balance for the overall radial stress at the free boundary. The volume-conserving solution, see equation (S40)–(S43), can satisfy the weak form of the radial force balance $\langle \sigma'_{rr} - p\rangle = -p_{\text{ext}}$ at $r = a$. On the other hand, our approximate solution, as explained above, ignores the exact boundary conditions at the free boundary in the pressurized phase, see equation (S31)–(S33), and thus does not obey the stress-free condition on the gel network $\sigma'_{rr} = 0$ at $r = a$, which is implied by the exact boundary conditions. This artifact of our approximate solution comes from ignoring the $M\partial_r(1/r)\partial_r rU$ term, implying we do not take into account the relaxations in the radial strain which are induced by $\sigma'_{rr} = 0$ and which are expected to occur, similar to the frictionless case, on a time scale $t_\parallel$. Therefore, we assume an approximate condition at the free boundary which interpolates between the weak form of the overall radial force balance in the volume-conserving phase and the weak form of the permeability condition, see equation (S33), in the pressurized phase, giving equation (S17). This approximate condition makes the contribution of the gel network to the radial stress vanish in the pressurized phase, thereby enforcing the weak form of the permeability condition in the pressurized phase. Using equation (S17), we then find $C = 2(1-T(t))G\epsilon + p_{\text{ext}}$. Similarly, we assume the force balance of the overall tangential stress at the free boundary, see equation (S32), to hold in weak form, i.e., $\langle \sigma'_{rz}\rangle = 0$ at $r = a$, which is satisfied trivially due to symmetry.

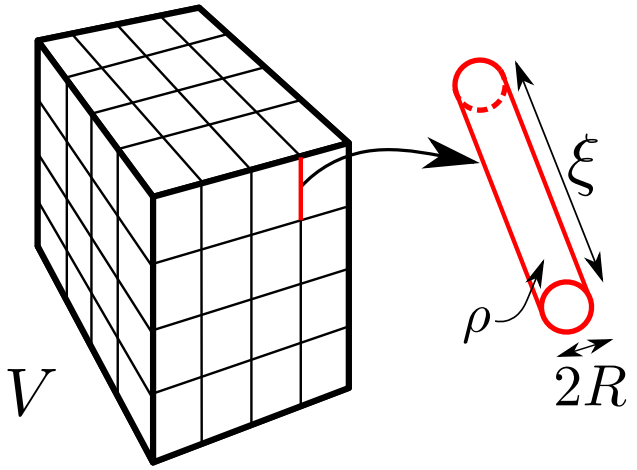

Fig. S2 In the cubic lattice model a fibrin network of volume V is modelled as a cubic lattice of fibrin fibers, where the edge length equals the mesh size ξ. The fibrin fibers have a radius R and mass density ρ.

S2 Cubic lattice model

During the polymerization of a fibrin fiber network fibrinopeptides are cleaved from fibrinogen molecules, thereby creating fibrin monomers. These monomers polymerize into protofibrils which in turn form fibrin fibers by both end-to-end and lateral aggregation[4]. To estimate the scaling of the permeability of a fibrin network with both the pre-polymerization fibrinogen concentration and large compressive strains on the network, we model the fibrin fiber network after polymerization as a cubic lattice.

S2.1 Mass conservation

Consider a volume V in which a fibrinogen solution with overall mass density c has been polymerized into a large number of cubic cells, forming a cubic lattice. Because of the large number of cells, the volume V can have any macroscopic shape. The cube edges have a length ξ, the mesh size, and consist of cylindrical fibrin fibers with radius R and fibrin monomer mass density ρ, see Figure S2. The total mass m of fibrinogen in the volume is $m = cV$. By mass conservation, the fibrinogen mass must be equal to the mass of fibrin monomers in the fibrin fibers, implying $m = \rho V_{\text{fiber}}$ with V_{fiber} the total volume of fibrin fibers, where we assume all fibrin monomers to be polymerized. As the mass of a fibrinogen molecule is about 340 kDa and the mass of the cleaved fibrinopeptides is about 1.5 kDa, we ignore the mass difference between a fibrinogen molecule and a fibrin monomer. Assuming the mesh size to be much larger than the radius R of the fibrin fibers, i.e., $\xi/R \gg 1$, the total volume of fibrin fiber can be expressed approximately as $V_{\text{fiber}} = L\pi R^2$, with L the total axial length of fibrin

#	c(mg/mL)	a (mm)	$\dot{\epsilon}$ (10^{-3}/s)	ϵ_e (%)	$k\left(10^{-1}\,\mu m^2\right)$	M (kPa)	G_0 (kPa)	ν (-)	$t_\perp/12$ (s)	M/GS^2
1	2	20	1.0	10	1.26(0.03)	1.45(0.12)	0.139	0.447(0.005)	3.3	0.026
2	2	20	1.0	10	4.97(0.19)	0.43(0.05)	0.142	0.257(0.039)	0.8	0.008
3	2	20	1.0	10	2.79(0.11)	0.91(0.09)	0.212	0.347(0.019)	1.0	0.011
4	2	20	1.0	10	1.73(0.03)	1.48(0.07)	0.087	0.469(0.002)	3.8	0.042
5	2	10	1.0	10	1.54(0.02)	0.15(0.01)	0.227	1.950(0.235)	1.6	0.007
6	2	20	1.0	5	5.00(0.33)	0.99(0.16)	0.119	0.431(0.013)	1.0	0.021
7	2	20	1.0	5	2.29(0.11)	1.28(0.26)	0.213	0.401(0.024)	1.2	0.015
8	4	20	1.0	10	2.17(0.08)	1.14(0.10)	0.444	0.181(0.048)	0.6	0.006
9	4	20	1.0	10	0.63(0.02)	3.43(0.34)	1.400	0.156(0.058)	0.7	0.006
10	2	20	5.0	10	1.20(0.07)	2.04(1.40)	0.162	0.457(0.032)	3.0	0.032
11	2	20	5.0	10	1.05(0.15)	0(4.10)	0.139	-	3.9	-
12	2	10	0.5	5	1.98(0.10)	0.30(0.04)	0.202	-0.562(0.418)	1.4	0.015
13	2	10	0.5	5	1.97(0.10)	0.36(0.04)	0.194	-0.071(0.133)	1.5	0.019
14	2	20	0.1	10	2.16(0.10)	0.27(0.01)	0.158	-0.184(0.075)	1.7	0.004
15	2	20	0.1	10	1.83(0.07)	0.30(0.01)	0.202	-0.537(0.132)	1.5	0.004

Table S1 Experimental conditions and fit results for compression experiments on large-pore fibrin gels at small strain. From the left to the right, the columns provide: the number tag given to each experiment, the concentration of fibrinogen c, the initial radius a of the gel before compression, the strain rate at which the gel is compressed $\dot{\epsilon}$, the amount of engineering strain put on the gel after compression ϵ_e, the fitted permeability k, the fitted longitudinal modulus M, the measured shear modulus just before compression G_0 from small-strain rheometry, the calculated Poisson's ratio $\nu = (M - 2G_0)/(2M - 2G_0)$, the exponential relaxation time $t_\perp/12$ with $t_\perp = h^2\eta/kG$ the pressurizing time, and the validity condition M/G_0S^2. All gels had an initial height of $h = 1$ mm and the estimation uncertainty is in brackets.

fiber in the volume. We then obtain

$$cV = \rho L \pi R^2, \tag{S46}$$

where $V = \xi^3 N$ and $L = 3\xi N$, since the unit cell of a cubic lattice contains three edges of a cube. We consider equation (S46) as an implicit function for ξ as a function of c, so a given overall fibrinogen mass density c results in a mesh size ξ after polymerization of the fibrinogen.

S2.2 Scaling laws

If the fibrinogen mass per unit of axial length $\pi R^2\rho$ depends on the fibrinogen concentration as $\pi R^2\rho \propto c^n$, we obtain $\xi \propto c^{(n-1)/2}$. And because the permeability is expected to scale as $k \propto \xi^2$, we find $k \propto c^{n-1}$. As reported in the manuscript, we find from experiments on small-pore fibrin gels that $k \propto c^m$, with $m = -2.2(0.5)$ and the uncertainty in brackets. This result implies that the fibrinogen concentration per unit of axial fiber length $\pi R^2\rho$ decreases with the overall fibrinogen concentration c. suggesting the polymerization kinetics to depend on c.

As the fibrin fibers are formed out of protofibrils, which in turn consist of fibrin monomers, one can express the mass of fibrinogen in the fibrin fibers as Nm_{proto}, with N the total number of protofibrils and m_{proto} the mass per protofibril. The protofibrils are formed by both end-to-end and lateral aggregation of fibrin monomers[4]. Therefore, the total number of protofibrils in the fibrin fibers can be calculated as $N = N_{\text{cross}}L/l_{\text{proto}}$, with N_{cross} the number of protofibrils per fibrin fiber cross-section, L the total axial length of fibrin fiber and l_{proto} the length of a protofibril. The mass balance then becomes

$$cV = \frac{LN_{\text{cross}}m_{\text{proto}}}{l_{\text{proto}}}. \tag{S47}$$

As the mass and length of a protofibril are both expected to be proportional to the number of fibrinogen monomers in the protofibril, we expect the ratio $m_{\text{proto}}/l_{\text{proto}}$ to be independent of the fibrinogen concentration c. Assuming the number of protofibrils per fiber cross-section to scale with fibrinogen concentration $N_{\text{cross}} \propto c^d$, we find that $k \propto \xi^2 \propto c^{d-1}$. Our finding that $k \propto c^m$, with $m = -2.2(0.5)$, thus implies that the number of protofibrils per fibrin fiber cross-section decreases with increasing fibrinogen concentration.

S2.3 Large compression

When a fibrin gel is under large compression, the vertically oriented fibers in the cubic lattic model will buckle. Assuming approximate homogeneous deformation, the vertical height of the buckled fibers is $\xi(1-\epsilon)$, where ϵ is the engineering strain. As fluid flows out of the gel radially, and since the permeability k is proportional to the surface area of the pores, we expect the permeability to scale as $k \propto \xi^2(1-\epsilon)$, giving the compression dependent permeability as $k(\epsilon) = k_0(1-\epsilon)$ with k_0 the permeability at zero strain. This strain-dependent permeability we use in equation (10) of the manuscript.

S3 Fit results

In section S1 the normal force exerted by a bonded disk-like gel under ramp compression was obtained from an approximate closed-form solution of the poroelastic equations of motion. Here, we analyze the compression experiments we performed on fibrin gels. By varying the experimental conditions, i.e., the amount of strain ϵ_e, the fibrinogen concentration c, the aspect ratio $S = a/h$ with the initial height h and radius a of the gel, and the strain rate $\dot{\epsilon}$, the microscopic response of the fibrin network will be reflected in the fitted elastic constants and the permeability. We use the Mathematica function `NonlinearModelFit` for fitting.

This journal is © The Royal Society of Chemistry [year]

We conducted experiments at body temperature on fibrin gels having either a large-pore fibrin network or a small-pore network. The large-pore gels have a typical mesh size ξ of about 1 micrometer[5,6]. The small-pore gels, on the other hand, have a mesh size of about a hundred nanometers. For the large-pore fibrin gels, compression experiments with both small and large strain have been conducted. In the small strain experiments the engineering strain, i.e., the ratio of the change in gap size over the gap size at polymerization, was maximally 10%. In the large strain experiments the fibrin gels were compressed up to 80% engineering strain in subsequent steps of 10% compression. For small-pore fibrin gels only small strain compression experiments up to 10% compression were conducted.

S3.1 Compression of large-pore fibrin gels

We conducted ramp compression experiments on large-pore fibrin gels under variable conditions in which we measured the normal force F exerted by the gel on the rheometer as a function of time t. See Figure S3 for an example of a compression experiment with relatively high strain rate and Figure S4 for a compression experiment with relatively low strain rate. These experiments were conducted with an initial gap size of $h = 1\,\mathrm{mm}$, and the standard conditions (SC) were chosen to be $\epsilon_e = 0.1$, $\dot{\epsilon} = 10^{-3}\,/\mathrm{s}$, $c = 2\,\mathrm{mg/mL}$ and $S = 20$. By varying one of these conditions relative to the experiments at standard conditions, the influence of the different conditions could be studied. After compression, the gel relaxes while the engineering strain is held constant. During and after compression the normal force exerted by the gel on the rheometer is measured. Moreover, just before the start of compression, the shear modulus G_0 of the gel is measured from small oscillation rheometry.

Comparing equation (S19) to the measured normal force, we fit the permeability k and the longitudinal modulus $M = K + 4G_0/3$. Table S1 gives the results for the fitted material parameters, the experimental conditions, and the exponential relaxation time. Moreover, we calculated M/G_0S^2 which, as shown in section S1, should be much smaller than unity to validly apply the approximate solution. Indeed, this is the case for all large-pore fibrin compression experiments.

From the measured shear modulus G_0 and the fitted longitudinal modulus M follows the Poisson's ratio of the gel network $\nu = (M - 2G_0)/(2M - 2G_0)$, where we assumed the ratio of the standard deviation in the measurement of the shear modulus to its measured value to be 1%. The uncertainties in G_0 and M are assumed to be independent because M was fitted against normal force measurements, while G_0 was inferred from a torsion measurement.

Next, we consider the influence of the different experimental conditions on the results for the permeability k and the Poisson's ratio ν.

S3.1.1 Compressive strain

The standard amount of engineering strain after compression of the gel is 10%. To probe the influence of strain, two compression experiments have been conducted with 5% strain instead, experiment 6 and 7. The standard condition (SC) experiments,

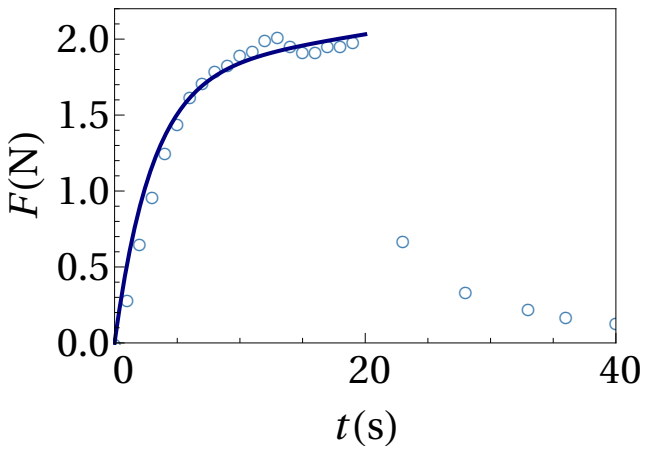

Fig. S3 The measured normal force F (blue circles) of a large-pore fibrin gel in response to fast ramp compression, see experiment 10 in Table S1 for the experimental conditions. The pressurizing time for the fluid pressure to build up to its maximal value is $t_\perp = 36$ s. The blue curve is a fit of equation (S19) to the measured normal force during compression, giving the permeability of the fibrin network k and its longitudinal modulus M as listed in Table S1.

experiment 1 t/m 4, give an average of the best estimates for the permeability of $\bar{k}_{SC} = 0.27(0.17)\,\mu\mathrm{m}^2$, with the standard deviation of the four best estimates in brackets. The uncertainty in the best estimate for each of the four individual experiments is smaller than 5%, see Table S1. Moreover, the average of the Poisson's ratio best estimates of the SC experiments is $\bar{\nu}_{SC} = 0.38(10)$, with individual uncertainty all less than 15%. We have four experiments at standard conditions, which is the highest number of repeated experiments within a single set of conditions in our data set. Since the individual uncertainties are much smaller than the standard deviation of the best estimates, we assume the standard deviation of the permeabilities and the Poisson's ratios to reflect the sample-to-sample variation among the different fibrin gels[7]. The variation probably arises from the nature of the polymerization process and the origin and purification process of fibrinogen.

The permeability estimates of the two 5% strain experiments are $k_6 = 0.50(0.03)\,\mu\mathrm{m}^2$ and $k_7 = 0.23(0.01)\,\mu\mathrm{m}^2$, with the uncertainty of the best estimate in brackets. The first of these two estimates is more than one standard deviation from the average of the standard condition experiments. Therefore, the 5% strain permeabilities measurements suggest that possibly the permeability for 5% strain is significantly different from a gel which is 10% compressed. The best estimates of the Poisson's ratio of the small strain experiments, however, are $\nu_6 = 0.43(0.01)$ and $\nu_7 = 0.40(0.02)$, which both lie within one standard deviation of the standard condition experiments. Therefore, the 5% Poisson's ratios suggest constancy of the Poisson's ratio in the range of 5-10% strain. Due to the small number of experiments, no conclusions can be drawn with respect to the influence of the magnitude of compression on k and ν.

S3.1.2 Concentration

The standard condition (SC) in the compression experiments takes a fibrinogen solution with mass concentration $c = 2\,\mathrm{mg/mL}$,

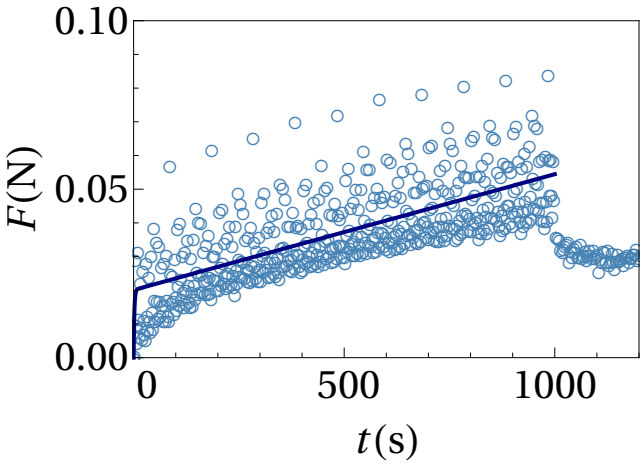

Fig. S4 The measured normal force F (blue circles) of a large-pore fibrin gel in response to slow ramp compression, see experiment 14 in Table S1 for the experimental conditions. The pressurizing time for the fluid pressure to build up to its maximal value is $t_\perp = 20$ s. The blue curve is a fit of equation (S19) to the measured normal force during compression, giving the permeability of the fibrin network k and its longitudinal modulus M as listed in Table S1.

see experiment 1 t/m 4. Two experiments were conducted with $c = 4\,\mathrm{mg/mL}$, experiment 8 and 9, to observe the influence of the concentration of fibrinogen. We expect a higher fibrinogen concentration c to give rise to a smaller mesh size ξ and thus a lower permeability k. Assuming the mass density per unit length of fibrin fiber to be independent of the fibrinogen concentration c, the cubic lattice model gives $k \propto c^{-1}$, see section S2.

With the scaling relation between the permeability and the mass concentration of the fibrin network, we turn to the fit results. Taking the average of the best estimates of the fitted permeability of the standard condition experiments, we find $\bar{k}_{\mathrm{SC}} = 0.27(0.17)\,\mu\mathrm{m}^2$, where in brackets is the standard deviation of the estimates, which we assume to measure the sample-to-sample variability of the permeability of different fibrin gels. The best estimates of the fitted permeability of the two 4 mg/mL gels are $k_8 = 0.217(0.008)\,\mu\mathrm{m}^2$ and $k_9 = 0.063(0.002)\,\mu\mathrm{m}^2$, with the uncertainty in brackets. Given the sample-to-sample variation of the permeability, one of the fitted permeabilities of the 4 mg/mL experiments does not lie within one standard deviation, suggesting that possibly the permeabilities of 4 mg/mL experiments differs significantly from the standard condition experiments. Given the scaling relation derived above and the permeability estimation from the standard condition experiments, we would expect the permeabilities of the 4 mg/mL gels to equal $\bar{k}_2/2 = 0.13(0.08)\,\mu\mathrm{m}^2$, with the sample-to-sample variation in brackets. The average of the two 4 mg/mL experiments is $\bar{k}_4 = 0.14\,\mu\mathrm{m}^2$, therefore pointing to the validity of the scaling relation.

Next, the fitted Poisson's ratio from the standard condition experiments is $\bar{\nu}_{\mathrm{SC}} = 0.38(0.10)$. The best estimates for the 4 mg/mL gels are $\nu_8 = 0.18(0.05)$ and $\nu_9 = 0.16(0.06)$, suggesting a significant difference in the Poisson's ratio. Due to the small number of experiments, however, no conclusions can be drawn on the influence of concentration on the permeability k and the Poisson's ratio ν.

S3.1.3 Geometry

To observe the influence of geometry, experiment 5 has been conducted, see Table S1, where the aspect ratio of the gel was $S = a/h = 10$ instead of $S = 20$ in the standard condition experiments. The fitted permeability of experiment 5 is $k_5 = 0.154(0.002)\,\mu\mathrm{m}^2$, whereas the standard condition experiments give an average permeability of $\bar{k}_{\mathrm{SC}} = 0.27(0.17)\,\mu\mathrm{m}^2$, with the standard deviation of the best estimates of the permeability of the standard condition experiments in brackets, which is presumed to measure the sample-to-sample variation in permeability. Therefore, the permeability of experiment 5 does not seem to be significantly different from the permeability with $S = 20$. The fitted Poisson's ratio of experiment 5 is $\nu_{10} = 2.2(0.3)$, because the longitudinal modulus M is fitted to be 160 Pa while the shear modulus G is 227 Pa, suggesting spontaneous contraction of the fibrin network. The reason for this awkward result is probably that the normal force increase during the pressurized phase is approximately 0.005 N, while the uncertainty in the rheometer measurements is about 0.01 N. Experiment 12 and 13 have also been conducted with an aspect ratio of $S = 10$, however, also having increases of the normal force during the pressurized phase of less than 0.01 N, but they do give physically reasonable fit values for the Poisson's ratio, $\nu = -0.56(0.42)$ and $\nu = -0.07(0.13)$, albeit with large uncertainties. Therefore, the anomalous value of the Poisson's ratio drawn from experiment 5 does not allow for a simple explanation.

S3.1.4 Strain rate

The standard strain rate is taken to be $\dot{\epsilon} \equiv v/h = 10^{-3}/\mathrm{s}$, with $v = 1\,\mu\mathrm{m/s}$ the velocity of the upper plate and $h = 1\,\mathrm{mm}$ the initial height of the sample. To observe the influence of strain rate, we conducted two experiments at $\dot{\epsilon} = 5 \cdot 10^{-3}/\mathrm{s}$, see Figure S3, and two at $\dot{\epsilon} = 0.1 \cdot 10^{-3}/\mathrm{s}$, see Figure S4. The standard condition (SC) experiments, experiment 1 t/m 4, yield an average permeability $\bar{k}_{\mathrm{SC}} = 0.27(0.17)\,\mu\mathrm{m}^2$, where the standard deviation due to sample-to-sample variability is between brackets. The high strain rate experiments, experiment 10 and 11, yield $k_{10} = 0.120(0.007)\,\mu\mathrm{m}^2$ and $k_{11} = 0.11(0.02)\,\mu\mathrm{m}^2$, which both fall within one standard deviation of the standard condition experiments. The low strain rate experiments, experiment 14 and 15, yield $k_{14} = 0.22(0.01)\,\mu\mathrm{m}^2$ and $k_{15} = 0.183(0.007)\,\mu\mathrm{m}^2$, both within the standard deviation of the standard condition experiments. Strain rate therefore does not seem to significantly influence the permeability of the fibrin network, as one would expect, because the permeability is expected to depend primarily on the microscopic structure of the fibrin network, see section S2.

The Poisson's ratio of the SC experiments yields $\bar{\nu}_1 = 0.38(0.10)$, and the high speed experiments, experiment 10 and 11, provide $\nu_{10} = 0.46(0.03)$ and $\nu_{11} = 1(14)$. Experiment 11 clearly gives an unreliable value for the Poisson's ratio. In this experiment the normal force decreases significantly during the pressurized phase, causing the fitted value of the longitudinal modulus to be fitted to zero, $M = 0(4)\,\mathrm{kPa}$, though the uncertainty indicates that M is in the order of kPa, similar to experiment 10. The Poisson's

This journal is © The Royal Society of Chemistry [year]

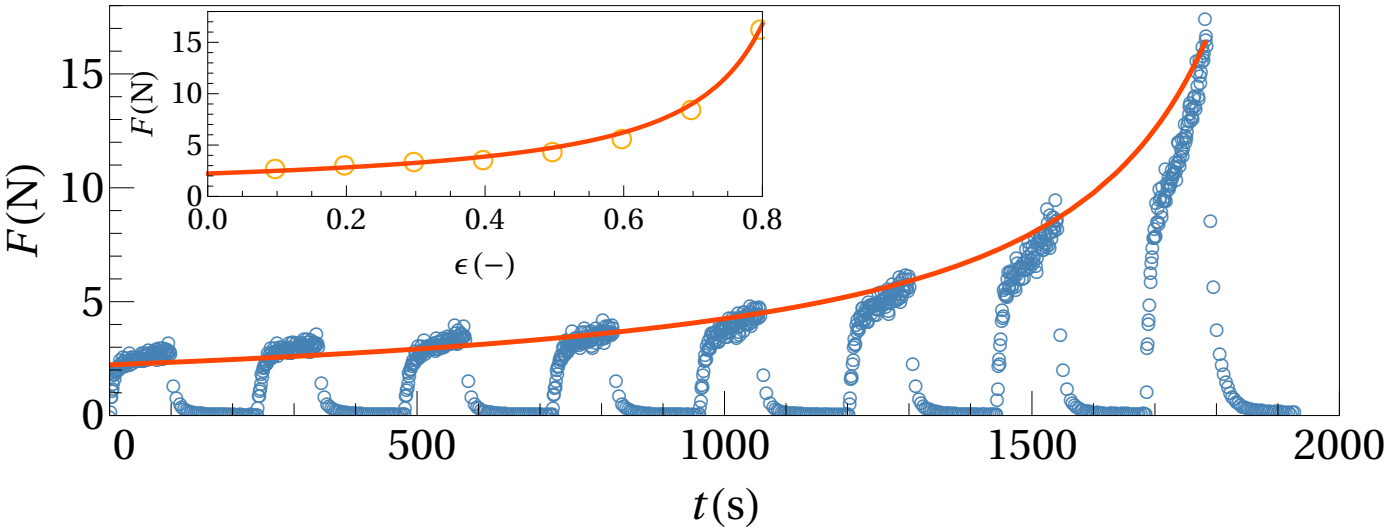

Fig. S5 The measured normal force F (blue circles) of a large-pore fibrin gel in response to eight consecutive ramp compression steps of 10% compressive strain each, see experiment 2 in Table S2 for the experimental conditions. The inset displays the maximal normal force during each compression step at the corresponding compressive strain (orange circles), which has been obtained by averaging the last 5% of data points of the compression step. The orange curve is a fit of equation (10) of the manuscript to the maximal normal force, giving the permeability of the fibrin network k_0 in the stress-free initial state and the proportionality constant of the Toll model b, as listed in Table S2.

#	c(g/L)	$\dot{\epsilon}$ (10^{-3}/s)	$k\left(10^{-1}\,\mu\text{m}^2\right)$	b (-)
1	4	1.0	0.180(0.030)	2.6(6.4)
2	4	1.0	0.195(0.008)	12.0(1.4)
3	2	1.0	0.682(0.048)	3.9(5.7)
4	2	1.0	1.070(0.050)	22.0(2.4)
5	2	5.0	1.510(0.068)	25.0(8.6)
6	2	5.0	1.400(0.029)	76.0(4.2)
7	2	0.1	1.020(0.031)	3.4(0.2)
8	2	0.1	0.943(0.045)	3.0(0.3)

Table S2 Experimental conditions and fit results for the large compression experiments ($\epsilon \leq 80\%$) on large-pore fibrin. From the left to the right the columns provide: the tag given to each experiment, the concentration of fibrinogen c, the strain rate at which the gel is compressed $\dot{\epsilon}$, the fitted permeability k, and the fitted proportionality constant of the Toll model[8] b. All gels have height $h = 1\,\text{mm}$ and radius $a = 20\,\text{mm}$ before compression, and the estimation uncertainty is in brackets.

ratio of experiment 10 falls within the variation of the SC experiments. The slow compression experiments, however, yield $\nu_{14} = -0.18(0.07)$ and $\nu_{15} = -0.54(0.13)$, clearly falling out of the sample-to-sample variation implied by the SCEs, see section 3.1 of the manuscript for interpretation of the strain rate dependence of the Poisson's ratio.

S3.2 Large compression of large-pore fibrin gels

Additional to the small strain experiments on large-pore fibrin gels, see section S3.1, large strain compression experiments on large-pore fibrin gels have been conducted to observe the fibrin fiber network response to large compressive strains. The standard experimental conditions were equal to that of the small strain experiments: the fibrinogen concentration in the gels was taken to be $c = 2\,\text{mg/mL}$, the applied strain rate was $\dot{\epsilon} = 1 \cdot 10^{-3}/\text{s}$, the initial gap size was $h = 1\,\text{mm}$ and the initial radius of the gel was $a = 20\,\text{mm}$. All gels were compressed up to 80% engineering strain in a stepwise fashion, see Figure S5. Each step comprised 10% strain and after each step the gel was allowed to relax, i.e., the measured normal force decreased after compression to a constant value. Figure S5 shows that the different compression steps have a similar normal force response, although the maximal normal force increases with compression. Therefore, we assume that also under large compression the gel enters the pressurized phase during compression.

In section S1, we assumed the gel network to be linear elastic, and to have a constant permeability, both rather poor assumptions for a fibrin gel under large compression. Therefore, as explained in section 2 of the manuscript, we assume a phenomenological form of the normal force as a function of the compressive strain in the pressurized phase, see equation (10) of the manuscript.

We assume the Young's modulus of a single fibrin fiber to be in the order of MPa: $E_\text{f} = 1\,\text{MPa}$[9]. The volume fraction of fibrin fiber before compression is $\phi_0 = fc/\rho_\text{fibrinogen}$, with $\rho_\text{fibrinogen} = 1.4 \cdot 10^3\,\text{kg/m}^3$ the mass density of pure fibrinogen[6], $f = 5.0$ the volume which a fibrin fiber encompasses relative to the volume of fibrinogen molecules in the fiber[10], and c the overall concentration of fibrinogen in the gel. As the fibrin fiber network sticks to the plates, one can approximate the average volume fraction as $\phi = \phi_0/(1-\epsilon)$, where we ignore the bulging of the gel since $S = a/h \gg 1$.

To fit equation (10) of the manuscript to the measured normal force in the pressurized phase, in principle one needs to know when the pressurized phase sets in. This is unknown outside of the linear regime.

As the exponential relaxation time in the first compression step is in the order of seconds, however, see Table S1, we assume that

#	c(g/L)	h (mm)	a (mm)	ϵ_e (%)	$k\left(10^{-3}\,\mu\mathrm{m}^2\right)$	M (kPa)	G_0 (kPa)	G_c (kPa)	t_c (s)	$t_\perp/12$ (s)
18	2	0.5	20	10	6.64(0.24)	6.1(2.7)	0.04	0.19(0.02)	6.4(0.6)	11
19	2	1.0	20	10	3.86(0.15)	0(4.6)	0.05	0.59(0.02)	7.9(0.3)	25
20	2	1.0	20	10	4.75(0.20)	0(4.1)	0.04	0.50(0.02)	7.9(0.3)	24
21	2	1.0	20	5	3.37(0.11)	-	0.05	0.49(0.01)	6.2(0.3)	35
22	2	1.0	20	5	3.40(0.13)	-	0.04	0.50(0.02)	6.7(0.3)	34
23	4	1.0	20	5	0.73(0.05)	-	0.24	1.03(0.02)	5.8(0.3)	77
24	4	1.0	20	5	0.73(0.06)	-	0.19	0.90(0.02)	9.3(0.2)	88
25	6	1.0	20	5	0.22(0.04)	-	0.47	1.22(0.03)	5.6(0.3)	211
26	6	1.0	20	5	0.30(0.04)	-	0.49	1.39(0.04)	5.9(0.3)	137
27	6	1.0	20	5	0.48(0.05)	-	0.36	1.08(0.03)	5.7(0.3)	110
28	6	1.0	10	5	0.80(0.07)	-	0.36	1.17(0.05)	10.8(0.4)	62
29	6	1.0	10	5	0.43(0.04)	-	0.40	1.99(0.07)	9.9(0.4)	68
30	6	1.0	10	5	0.74(0.06)	-	0.49	1.36(0.05)	9.9(0.4)	57
31	8	1.0	20	5	0.22(0.03)	-	0.65	1.69(0.04)	7.2(0.3)	152
32	8	1.0	20	5	0.16(0.04)	-	0.70	1.24(0.03)	9.8(0.4)	295
33	10	1.0	20	10	0.17(0.05)	-	0.97	1.32(0.05)	14.4(1.0)	264

Table S3 Experimental conditions and fit results for compression experiments on small-pore fibrin gels. From left to right, the columns provide: the tag given to each experiment, the concentration of fibrinogen c, the initial height h and radius a of the gel before compression, the strain rate at which the gel is compressed $\dot{\epsilon}$, the amount of engineering strain put on the gel after compression ϵ_e, the fitted permeability k, the fitted longitudinal modulus M, the measured shear modulus just before compression G_0 from small-strain rheometry, the augmented shear modulus during compression G_c, and the exponential relaxation time $t_\perp/12$ with $t_\perp$ the pressurizing time. The strain rate is $\dot{\epsilon} = 10^{-3}\,/\mathrm{s}$ in all experiments, and the uncertainty is given in brackets.

at the end of each compression step, with $t_e = 20100\,\mathrm{s}$, the gel has entered the pressurized phase, and we fit equation (10) of the manuscript to the maximal normal forces. Due to the uncertainty in the measured normal force, we take the last five percent of data points of a given compression step and average both the normal force and the strain of the different data points, to obtain a single data point per compression step, see the inset of Figure S5.

Two of the large compression experiments were performed at standard conditions, two at high strain rate $\dot{\epsilon} = 5 \cdot 10^{-3}\,/\mathrm{s}$, two at low strain rate $\dot{\epsilon} = 0.1 \cdot 10^{-3}\,/\mathrm{s}$, and two with a doubled concentration of fibrinogen $c = 4\,\mathrm{mg/mL}$, see Table S2. Comparing experiment 1 and 2 to experiment 3 and 4, the fitted prefactors b do not appear to be influenced by the fibrinogen concentration c. This result confirms the assumed form of the stress response of the fibrin fiber network as that of a randomly structured fiber network in the Toll model[8], where the concentration of fibrinogen is taken into account by the volume fraction of fibrin fibers ϕ. Comparison of experiment 3-8, where the influence of strain rate is probed, suggests a monotonous increase of b with the strain rate, see Figure 4 of the manuscript. This increase is analogous with the findings described in section S3.1.4, which showed that for higher strain rate the gel responds more like a volume-conserving solid. The increase in strain rate suggests that for the strain rate going to zero the proportionality constant b of the fiber network response could be of order 1 or less. The dependence of the normal force to strain rate in large compression experiments shows that the strain rate dependence of the mechanical response of the fibrin fiber network holds both for small and large compressive strain.

Next, as noted in section S3.1.2, we expect the permeability to scale as $k \propto c^{-1}$, and we do not expect it to depend on the strain rate, which determines the fluid velocity through the fiber network, as the permeability is supposed to be determined by the architecture of the network. The network architecture would depend on the amount of compressive strain, but not on the strain rate. Therefore, we expect the fitted permeability at zero compression k_0 to be independent of the strain rate, although we do expect sample-to-sample variation, see section S3.1.1. Experiment 3-8 provide permeabilities which indeed fall within approximately one standard deviation of the permeability of experiment 1-4 of the small strain experiments under standard conditions, see Table S1 and S2. All fitted permeabilities are at the lower end, however, which seems somewhat unexpected. Moreover, given the scaling relation $k \propto c^{-1}$, the permeability of experiment 1 and 2 with $c = 4\,\mathrm{mg/mL}$ would be expected to be approximately half of that of experiment 3-8. This is not confirmed by the fitted values, however. Due to the low number of experiments no conclusions can be drawn.

S3.3 Compression of small-pore fibrin gels

Next to the compression experiments on large-pore fibrin gels, see section S3.1, gels of small-pore fibrin networks have been compressed while measuring the normal force. The standard conditions were, similar to those in section S3.1 and S3.2, a fibrinogen concentration of $c = 2\,\mathrm{mg/mL}$, a strain rate of $\dot{\epsilon} = 10^{-3}\,/\mathrm{s}$, an initial gel height of $h = 1\,\mathrm{mm}$, and an initial radius of $20\,\mathrm{mm}$. We increased the concentration of fibrinogen up to 10 mg/mL to observe its influence on the permeability. Moreover, we varied the geometry of the gels to test the validity of the approximate solution presented in section S1. Below, we first discuss the numerical details of the fitting procedure. Afterwards, we consider the influence of fibrinogen concentration and geometry on the permeability and shear modulus of small-pore fibrin networks.

This journal is © The Royal Society of Chemistry [year]

S3.3.1 Strain stiffening

As noted in section 2 of the manuscript, we accommodate for strain stiffening by replacing $Gt \rightarrow \int_0^t G(t')\,\mathrm{d}t'$ where G enters in equation (S19), with $G(t)$ as given in equation (7) of the manuscript. For the numerical fit routine, we use a sigmoidal function with very high power $n = 33$ to interpolate approximately stepwise and analytically from G_0 to the augmented shear modulus G_c. This gives for the time-dependent shear modulus

$$G(t) = G_0 + (G_c - G_0)\,\frac{(t/t_c)^n}{1 + (t/t_c)^n}. \qquad \text{(S48)}$$

All small-pore fibrin experiments can be described well by fitting the permeability k, the augmented shear modulus G_c, the onset time for strain stiffening t_c, and, if possible, the longitudinal modulus M, see Table S3.

In experiment 18, the fit routine was able to converge with a meaningful value of the longitudinal modulus $M = 6.2(2.7)\,\mathrm{kPa}$. The reason for convergence is that in this experiment the initial height of the gel was $h = 0.5\,\mathrm{mm}$, causing a relatively short exponential relaxation time $t_\perp/12 = h^2\eta/12kG_c$ of 11 s. Therefore, during a significant portion of compression the gel is to good approximation in the pressurized phase, in which the increase in normal force is solely due to the longitudinal modulus, see equation (S19). For experiment 21-33, we put $M = 0$ by hand, because otherwise the fit routine does not converge. This presumption is also justified, however, for the following reasons. Arguably, the non-convergence is due to the negligible effect of the mechanical response, $\pi a^2 M\epsilon_e$ with a the initial radius of the gel and ϵ_e the amount of strain after compression, in the pressurized phase. Moreover, these experiments all have $h = 1\,\mathrm{mm}$, implying a longer pressurizing time than in experiment 18. In part of the experiments, the gel is compressed with only 5% engineering strain $\epsilon = 0.05$, reducing the mechanical response contribution even further. Finally, with increasing concentration the relaxation time $t_\perp$ seems to increase, thereby increasing the time needed to enter the pressurized phase and decreasing the influence of M, see Figure S6 for a high fibrinogen concentration experiment with $M = 0$.

S3.3.2 Concentration and geometry

To observe the influence of the concentration of fibrinogen c we conducted experiments with $c = 2, 4, 6, 8, 10\,\mathrm{mg/mL}$, see Table S3 for the results and Figure S6 for a high fibrinogen gel. The permeability k decreases with increasing fibrinogen concentration c, see Figure (7) of the manuscript.

Up to the increase of the shear modulus at t_c, the fibrin gels deform in an approximately volume-conserving manner. Therefore, the compression up to $t = t_c$ can be considered as a shear deformation of the sample. The tangential radial stress at the sample-plate interface therefore shears the sample. Within the gel the shear stress is lower because the gel can bulge out. The tangential stress at the sample-plate interface before stiffening is given as $\sigma_{n,rz} = G_0\,(\partial_z U + \partial_r W) = G_0\partial_z U$, since W is independent of r, as we presumed in this entire analysis. The radial deformation U grows linearly with the radial coordinate r, see equation (S1). Therefore, we average the tangential stress over the gel plate interface to obtain the onset stress:

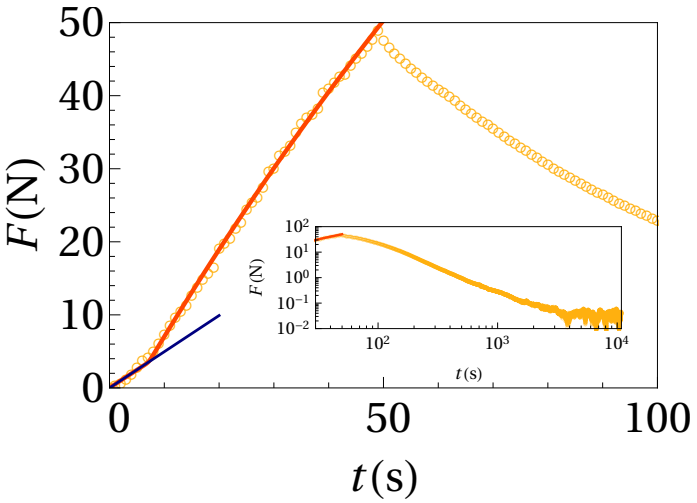

Fig. S6 The measured normal force F (orange circles) of a small-pore fibrin gel with high fibrinogen concentration, see experiment 31 in Table S3 for the experimental conditions. The pressurizing time for the fluid pressure to build up to its maximal value is $t_\perp = 1824\,\mathrm{s}$. The orange curve is a fit of equation (S19) to the measured normal force during compression, giving the permeability of the fibrin network k, the onset time of strain stiffening t_c and the augmented shear modulus G_c as listed in Table S3. Before the onset time of strain stiffening, the normal force follows the time dependence expected for a volume-conserving solid with the measured initial shear modulus G_0. The inset shows an extended process of gel relaxation after compression stops.

$\sigma_c \propto \left(1/\pi a^2\right) \int_0^a \mathrm{d}r\, 2\pi r \sigma'_{rz}|_{z=h,t=t_c}$, giving equation (9) of the manuscript, and the dependence of σ_c on the concentration of fibrinogen c is given in Figure 6 of the manuscript.

Experiments 25-30 have a fibrinogen concentration of $c = 6\,\mathrm{mg/mL}$, whereas experiments 25-27 have an initial radius of $a = 20\,\mathrm{mm}$ and experiments 28-30 have $a = 10\,\mathrm{mm}$. According to equation (S19), a difference in the magnitude of the normal force $F_N \propto a^4$ is to be expected, but no difference in the fitted permeability k, the shear modulus G_c and the critcial time t_c. The three fit parameters are all of the same order, their differences are probably due to sample-to-sample variation, and the coefficient of determination exceeds 0.9992 for every experiment. Therefore, our model seems to account correctly for the influence of geometry.

S3.4 Shear modulus

In section S3.1 we found the measured normal force in all large-pore fibrin compression experiments during compression to be explained by the approximate solution of section S1, while using the measured value of the shear modulus G_0 just before compression. For small-pore fibrin gels, however, we found the shear modulus to increase at an onset stress and to remain constant afterwards. In this section, we also consider the evolution of the shear modulus after compression.

For large-pore fibrin gels undergoing large compression, see section S3.2, the shear modulus has been measured before and after compression, see for example Figure S7. Before compression, the shear modulus has a constant value G_0. After compression,

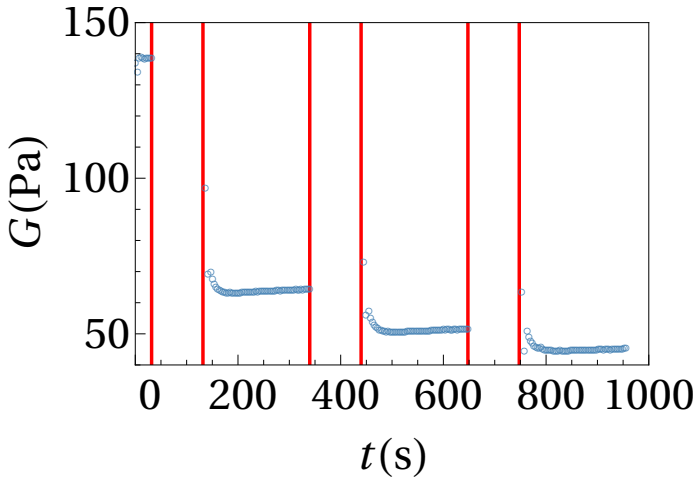

Fig. S7 The measured shear modulus G (blue dots) before and after three compression steps of 10% compressive strain for a large-pore fibrin sample. The beginning and end of a compression step are denoted by a red line. Before each compression step the shear modulus is (approximately) constant. After each step the shear modulus decreases rapidly to a smaller value than before compression.

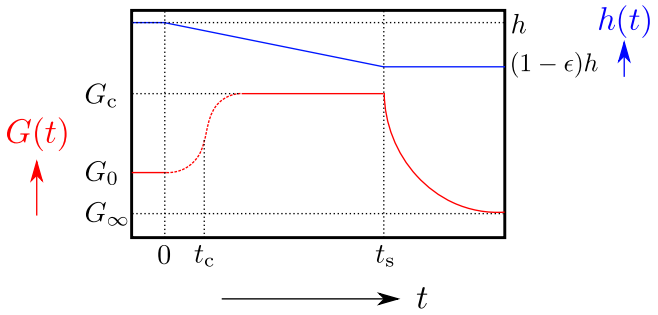

Fig. S8 Schematic of the development of the shear modulus $G(t)$ in response to changes in the height $h(t)$ of a ramp-compressed fibrin gel during and after compression. Initially, for $t < 0$ the shear modulus has magnitude G_0. As compression commences, the shear modulus increases to G_c, with the point of maximum increase at the onset time t_c. The difference between G_c and G_0 is negligibly small for large-pore fibrin gels but may be significant for small-pore fibrin gels. This difference is probably due to the much shorter volume-conserving phase of large-pore fibrin gels. After compression stops at t_e, the shear modulus decreases to its static value G_∞, which is determined by the compressive strain.

it first decreases rapidly. Subsequently, it increases very slowly and can be regarded as approximately constant, i.e., as if the gel is relaxed. Just after compression, the shear modulus seems to be at approximately the same value as before compression, suggesting the shear modulus in large-pore fibrin gels to be approximately constant during compression, as we assumed in section S3.1. With each compression step, the magnitude of the relaxed shear modulus is decreased compared to its value before compression, in accordance with literature [11].

Combining the results from section S3.1, S3.3 and the shear modulus measurements just after compression, we can form a coherent picture of the evolution of the shear modulus during and after the compression of fibrin gels, see Figure S8. Before compression, the gel has a constant shear modulus which reflects that the gel is in equilibrium. As soon as compression starts it is first compressed in a volume-conserving manner because the (low) permeability of the gel prevents fluid to be squized out instantaneously. In this phase the shear modulus may increase around an onset stress σ_c in the network, see equation (9) of the manuscript. If fluid starts to flow out before the gel is stressed to σ_c, the shear modulus remains constant throughout the whole of the ramp compression, as with the large-pore compression experiments in section S3.1. If σ_c is reached while being in the volume-conserving phase, the shear modulus can increase significantly and remains so during the rest of compression, see section S3.3. After compression, the shear modulus relaxes to its static value.

Possibly, these results can be interpreted as follows. For the small-pore fibrin gels, as the gel is compressed in a volume-conserving manner, the fibers are pulled increasingly straight in the lateral direction, until they are pulled taut, and afterwards they are pulled further in tensile deformation. The fibers are pulled taut around the onset stress, causing the shear modulus to increase accordingly. Note that in our approximate solution the shear modulus only measures the resistance of the network due to bulging of the network, that is, to radial curvature of the network, encoded in the $G\partial_z^2 U$ term in the force balance. Indeed, this resistance can increase when the fibers become aligned in the lateral direction, because the aligned fibers are connected perpendicularly to the lateral direction. After compression stops, the fluid pressure which has built up during compression, mainly due to stretching of the straightened fibers, pushes fluid out of the network which makes the network contract laterally, thereby decreasing the tension in the fibers and the magnitude of the normal force.

For the large-pore fibrin gels, the volume-conserving phase is very short, and in the pressurized phase the fibers are probably aligned due to the fluid velocity, that is, the alignment increases with the rate of compression. In our analysis of the large-pore fibrin gels we assume the shear modulus to be equal to the measured shear modulus before compression G_0, even though alignment would increase the shear modulus, similar to the increase in the shear modulus G for the small-pore gels. This simplifying assumption only influences the description of the short time exponential relaxation through the pressurizing time $t_\perp = h^2\eta/kG$. This relaxation, however, is apparently well approximated by taking G equal to the measured shear modulus G_0. In the pressurized phase, the elastic response of the network to the normal force is given by the longitudinal modulus M. Alignment of the fibrin fibers thus translates in an increase of the value of the fitted longitudinal modulus, or equivalently the calculated Poisson's ratio, with increasing compression rate, see Figure 4 and 5 in the manuscript. The measured shear modulus just after compression is approximately equal to the measured shear modulus before compression. Probably, this is because the shear modulus is measured by small-angle shear rheology which may experience only little influence from alignment of the fibers in the radial direction. After compression, when the network relaxes into its static conformation, the measured shear modulus decreases to its static value as the fiber network relaxes due to fluid outflow, see Figure

This journal is © The Royal Society of Chemistry [year]

S7.

References

1 C. G. Armstrong, W. M. Lai and V. C. Mow, *Journal of Biomechanical Engineering*, 1984, **106**, 165–173.

2 S. Qiao and N. Lu, *International Journal of Solids and Structures*, 2015, **58**, 353–365.

3 T. Yamaue and M. Doi, *Physical Review E - Statistical Physics, Plasmas, Fluids, and Related Interdisciplinary Topics*, 2004, **69**, 5.

4 J. W. Weisel and R. I. Litvinov, *Fibrous Proteins: Structures and Mechanisms*, Springer International Publishing, 2017, vol. 82, pp. 405–456.

5 H. C. De Cagny, B. E. Vos, M. Vahabi, N. A. Kurniawan, M. Doi, G. H. Koenderink, F. C. MacKintosh and D. Bonn, *Physical Review Letters*, 2016, **117**, 1–5.

6 C. Yeromonahos, B. Polack and F. Caton, *Biophysical Journal*, 2010, **99**, 2018–2027.

7 M. Pieters, A. Undas, R. Marchi, M. P. M. De Maat, J. W. Weisel and R. A. S. Ariëns, *Journal of Thrombosis and Haemostasis*, 2012, **10**, 2179–2181.

8 S. Toll, *Polymer Engineering and Science*, 1998, **38**, 1337–1350.

9 J.-P. Collet, H. Shuman, R. E. Ledger, S. Lee and J. W. Weisel, *Proceedings of the National Academy of Sciences*, 2005, **102**, 9133–9137.

10 M. E. Carr and J. Hermans, *Macromolecules*, 1978, **11**, 46–50.

11 A. S. G. van Oosten, M. Vahabi, A. J. Licup, A. Sharma, P. A. Galie, F. C. MacKintosh and P. A. Janmey, *Scientific Reports*, 2016, **6**, 1–9.